Generation and Interpretation of Synthetic Photon Energy Spectra Based on a Photospheric Model of Gamma Ray Burst Emission

Arman Aspromonti
arman.aspromonti@gmail.com

under the direction of
Filip Samuelsson
Division of Particle and Astroparticle Physics
Department of Physics
KTH Royal Institute of Technology

Research Academy for Young Scientists
July 14, 2021

Abstract

Gamma-ray bursts (GRBs) are the result of supernovae or binary neutron star systems collapsing under gravity while rotating at high speeds, ejecting jets of plasma. However, there is currently no scientific consensus on a clearly defined model that can describe their behaviour. Thus, this paper aims to gain a better understanding of a model based on photospheric GRB emission, which is one kind of model that can be used to describe GRBs. The model is used to generate synthetic photon energy spectra representing simulated GRBs which are then processed and fit with a mathematical function known as the Band function. By varying one of the three variables included in this model and observing changes in a parameter of the Band function, conclusions were drawn about how GRB parameters affect the perceived shape of observed spectra. It was ultimately concluded that although a mathematical relationship can be found between two parameters, it was affected by external factors to an uncertain degree. Future studies may be required to find a more generally applicable relationship.

Acknowledgements

First of all, I would like to thank Rays - for Excellence and their collaborators, Kjell & Märta Beijers Stiftelse and Kungl. Patriotiska Sällskapet, for allowing me to participate in this wonderful project. More specifically, I would like to thank the organisers Max Kenning, Miranda Carlsson, Ann-Kristin Malz and Markus Swift for their invaluable encouragement and guidance. Secondly, I would like to thank my supervisor Filip Samuelsson for teaching me everything I know about gamma-ray bursts and helping me gain insight into one of the most interesting and engaging niches in physics. Further, I extend my gratitude to my research partner Elliot Hansson for always challenging my understanding of the topic and opening my mind to new approaches. Lastly, I am thankful to my family for keeping contact with me and supporting me through the research process.

Contents

1 Introduction

Gamma-ray bursts (GRBs) have been described as "the most luminous and mysterious explosions in the universe" [1]. These events are the result of supernovae or binary neutron star systems collapsing under gravity while rotating at high speeds, ejecting jets of plasma, charged particles and high energy photons. However, there are many aspects of GRBs that are unclear or unknown. One such aspect is the source of the perceived gamma-rays. There is currently no scientific consensus on a clearly defined model that can describe GRB emission, which has presented a major gap in the understanding of astroparticle physics. [2]

To remedy this, a number of theories explaining this have been posited, such as the photospheric model of GRB emission that this paper focuses on. By using a mathematical model to generate synthetic GRB data and analysing that data in the same way real GRBs are investigated, this paper hopes to draw conclusions about the properties of real GRBs under the assumption that the model can accurately describe them.

1.1 Theory

The main type of GRB data that this paper will focus on is photon energy spectra, hereby referred to as spectra. A spectrum is simply a distribution of the number of detected photons and their energies, typically measured in eV. Any model that deals with GRBs must be able to explain why the spectra of GRBs look the way they do.

Another important concept is optical depth, τ, which represents the likelihood that a photon is absorbed or otherwise interacted with. Optical depth relates to transmittance (T), the percentage of radiant energy not lost to absorption, according to the relationship $T = e^{-\tau}$. [3]

For each photon, T represents the likelihood that it will not be absorbed, and thus the probability of it escaping. Initially, the GRB outflow will be too optically thick and most photons will be absorbed, but as it travels further and the jet widens, τ will be low

enough to allow photons to escape. The point at which $\tau = 1$ and T is approximately 37% is referred to as the photosphere. [1]

All models of GRB emission include a photosphere, but they differ in what gives the photons in a GRB the energies observed. In a standard photospheric model, the radiation exiting the photosphere is expected to have reached thermal equilibrium, meaning that the resultant spectrum would resemble a blackbody. However, GRB spectra do not resemble blackbodies, which implies that there are other processes that lead to photons energising more than expected [4]. In the model this paper investigates, those processes are subphotospheric radiation-mediated shocks (RMSes), which occur when faster parts of the GRB jet collide with slower ones, leading to energy exchange between charged particles and photons within the collision.

1.1.1 The Compactness Problem

One aspect of GRBs that all models must take into account is the fact that they travel towards the point of observation relativistically (approaching the speed of light). This can be deduced from what is referred to as the compactness problem. When light travels to Earth from a spherical shell, such as the photosphere of a GRB, light coming from different parts of the sphere will be observed at different times due to its curvature. This time delay allows for the radius of the sphere to be calculated. However, for the shortest GRBs of $\sim$ 10 ms, this yields radii so small that photons at the observed energies are dense enough to split into electron-positron pairs in a process known as pair production. As this is not observed, it is assumed that the jet of the GRB is travelling towards Earth at relativistic speeds. This would cause the frequency of each photon to blueshift due to the Doppler effect, where the perceived frequency of a photon increases if the source of the photon is travelling towards the point of observation, meaning that the energy of the photons in their rest frame is not high enough for pair-production. [5, 6]

1.1.2 Photon Emission Mechanisms

In GRBs and other similar phenomena, there are a number of emission mechanisms that lead to the radiation of photons and affect their energies. In this paper, the most prevalent emission mechanism is *Bremsstrahlung*, a phenomenon in which the trajectory of an electron is slightly altered by a positively charged particle such as a proton, thus decelerating it. In accordance with the law of conservation of energy, the excess energy is emitted as a photon. Another emission mechanism is synchrotron radiation, which is similar to *Bremsstrahlung*, but occurs when electrons moving at relativistic speeds are decelerated by magnetic fields. [7, 8]

Lastly, an important mechanism by which photons can gain or lose energy is Compton scattering. When a photon collides with a stationary charged particle such as an electron or positron, the photon will be deflected, resulting in energy loss for the photon as seen in figure 1. If the target particle is moving with sufficient speed, on the other hand, the photon may receive energy in a process called inverse Compton scattering. Repeated Compton scatterings redistribute photon energies in what is known as Comptonisation, altering spectra to resemble blackbodies as the photons approach thermal equilibrium. [9]

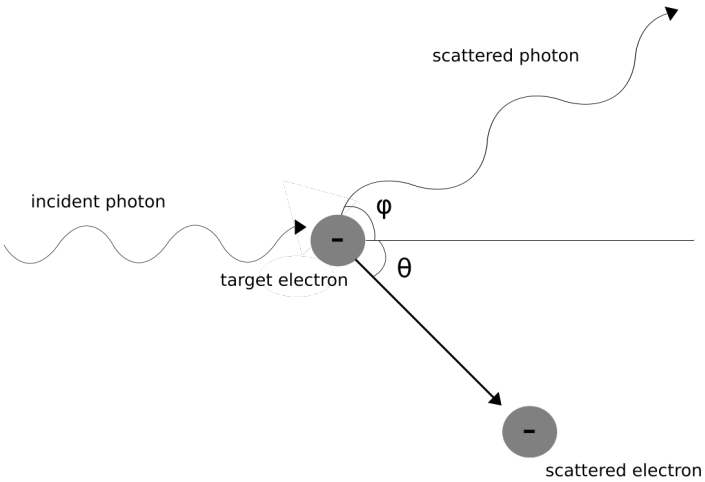

Figure 1: A visualisation of Compton scattering. In this figure, ϕ and θ are angles for the trajectories of the photon and electron relative to the original path of the photon after scattering.

1.1.3 Radiation-Mediated Shocks

In simple terms, a radiation-mediated shock occurs when a segment of the GRB outflow travels faster than the ejecta ahead of it, leading to a collision. These shocks can be divided into three distinct zones: Upstream, RMS and downstream. The upstream zone is the part of the jet that travels faster than the downstream, colliding into it. The RMS zone is the point of contact between the upstream and downstream, where the shock itself occurs. Here, the upstream rapidly decelerates relative to the shock upon contact with the downstream, allowing photons from upstream to engage in Compton scatterings with high energy electrons within the shock and gaining the highest energies observed. After decelerating, the upstream merges with the downstream as it travels towards the photosphere. [10]

Though Compton scatterings tend towards a blackbody function, Comptonisation occurs at different energies in all three zones of the RMS, leading to the observed spectrum. Scatterings in the upstream zone will form a blackbody around the temperature θ_{U}, while the high energy of the shock causes photons in the RMS zone to Comptonise around the much higher temperature θ_{R}. The presence of photons that both have and have not gained higher energy in the RMS zone thus leads to a blackbody spectrum somewhere between upstream and RMS in the downstream, at the energy θ_{C}. Hence, the spectrum of a GRB can be described by three superimposed blackbody spectra, see figure 2. [10]

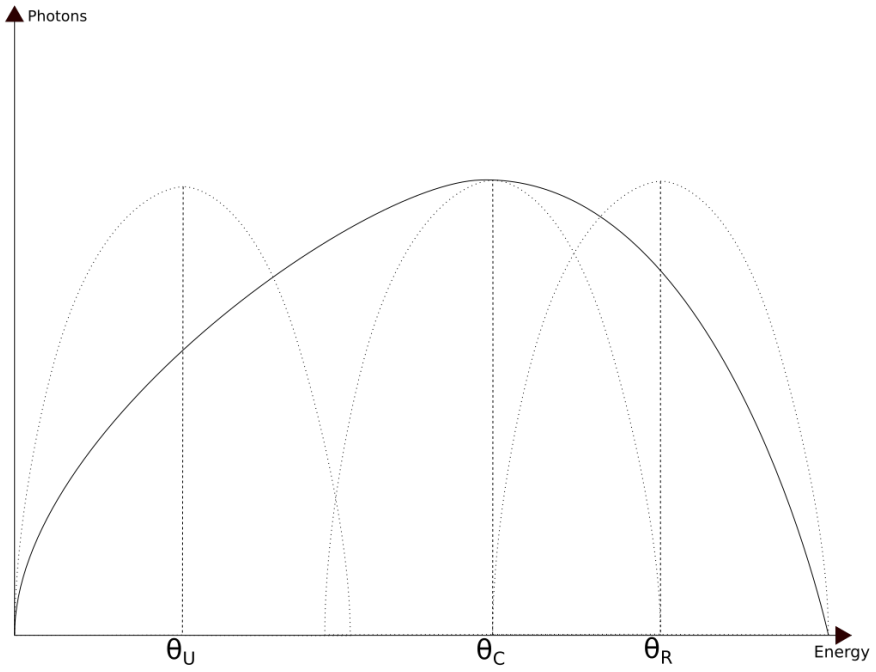

Figure 2: An illustration of how Comptonisation at different temperatures affects the shape of the spectrum. The dotted lines represent the blackbody spectra that photons tended towards in each zone of the RMS.

Due to the similarities between Compton scattering in the different zones of the RMS and thermal Comptonisation, the mathematical model analysed in this study is based on the Kompaneets equation, which describes the latter [11]. Combined with radiation-mediated shocks, this forms the name Komrad. Thus, the model will henceforth be referred to as Komrad.

1.2 The Band Function

Historically, the most common way to fit GRB data is using the Band function. It is a broken power law function, meaning that it describes curves as a positive power law which peaks at a certain point and then descends with a second, negative power law. The Band function has three parameters α, β and E_0, representing the first and second power laws and the peak of the function respectively. These parameters are used to define the number of photons N_{ph} as a function of energy E, see equation (1).

$$N_{\mathrm{ph}}(E) = A \begin{cases} (\frac{E}{100\mathrm{keV}})^{\alpha} \exp\left(-\frac{E}{E_0}\right) & E < (\alpha - \beta)E_0 \\ (\frac{E}{100\mathrm{keV}})^{\alpha-\beta} \exp(\beta - \alpha)(\frac{E}{100\mathrm{keV}})^{\beta} & E \geq (\alpha - \beta)E_0, \end{cases} \tag{1}$$

in which A is the normalisation factor that depends on the distance and brightness of the GRB. In all GRB data so far, values of α have ranged from -2 to 0, but are most common in the -1 to -0.5 range. Correspondingly, values of β have ranged from -3.8 to -1.3 but are most common between -2.3 and -1.6, and E_0 has historically varied from $30 - 1000$ keV but is most often seen in the $100 - 200$ keV range. [12]

2 Method

This study used the aforementioned mathematical model, Komrad, to simulate the effects of a subphotospheric radiation-mediated shock on photon energies in a GRB and produce synthetic spectra. These spectra were then processed by adding random noise and altering the spectra to simulate how the synthetic GRBs would appear as observed by the Fermi Gamma-ray Space Telescope. The Band function was subsequently fit to these spectra, as is typically done to define the shapes of GRB spectra [12]. With this experimental setup, observing changes in the parameters of the Band function in relation to changing the variables of Komrad gave insight regarding how the shapes of spectra were affected by the various factors taken into account by the model.

2.1 Generation of Synthetic Spectra

The generation of synthetic spectra was divided into two phases. In the first phase, Komrad was used to generate template spectra from a set number of possible values for each of its three parameters. Synthetic spectra were then drawn for any values in between those of the template spectra, using their shapes as a point of reference. In the second phase, noise was added to these spectra in the form of randomisation and a function

representing background radiation. Additionally, the spectra were adjusted to match the response of a node on the Fermi Gamma-ray Space Telescope, meaning that the photon energies were altered based on which energies are within the observational window of the telescope and depending on variations in the sensitivity of each node to certain energy bands.

2.1.1 Parameters

In Komrad, the shapes of spectra are determined by three parameters: $\tau\theta$, R and Y_R. R is the ratio between the temperature of the RMS, θ_R, and the temperature of the upstream photons, θ_U. This represents the difference between the energies of the high energy photons and the low energy photons, thus affecting the length of the spectrum. Y_R is effectively how much time the photons spend inside the RMS zone during a shock. Larger values of Y_R represent a higher degree of Comptonisation in the high energy band as the photons have time to scatter with high energy electrons in the shock. Therefore, Y_R affects the number of photons with high energy and thus the gradient of the spectrum, with a Y_R of 1 indicating a flat shape. $\tau\theta$ is a combined parameter consisting of two variables, the optical depth τ and the temperature of the shock θ_R. Because optical depth is a measure of how likely photons are to interact with other particles, it can be used as the likelihood for Compton scattering. The temperature then determines how much energy is donated or received by photons in these scatterings. It follows that $\tau\theta$ is a measure of how much the spectrum moves towards thermal equilibrium downstream, after the shock has occurred but before the photons reach the photosphere. The effects of varying these parameters on the shapes of spectra is illustrated in figure 3.

In this study, Komrad was used to generate 125 template spectra for a number of possible combinations of these three variables. Artificial spectra were then created for any values of $\tau\theta$, R and Y_R by drawing spectra based on the templates, see figure 4.

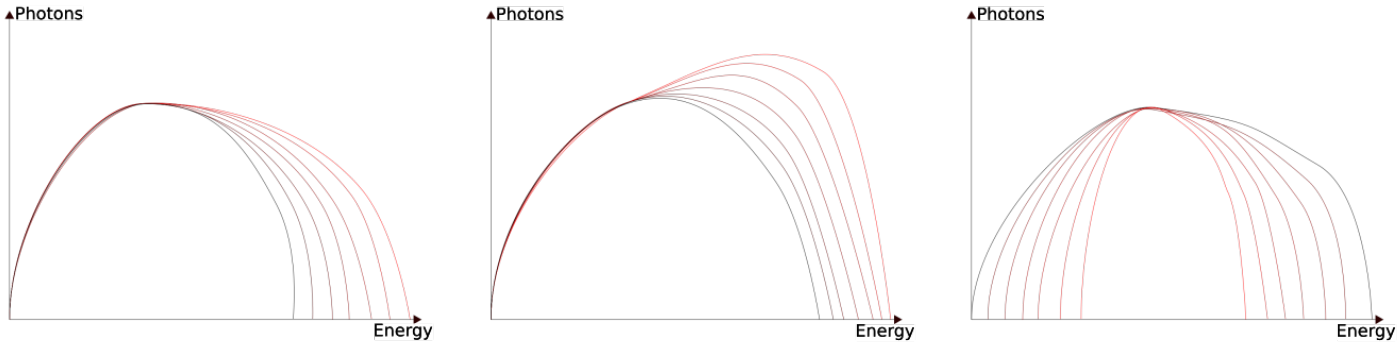

(a) Varying R. (b) Varying Y_R. (c) Varying $\tau\theta$.

Figure 3: Rough illustrations showing how varying R, Y_R and $\tau\theta$ respectively should affect spectra. As $\tau\theta$ is the least intuitive variable, impossibly high values of it were used to show how spectra approach thermal equilibrium as it increases.

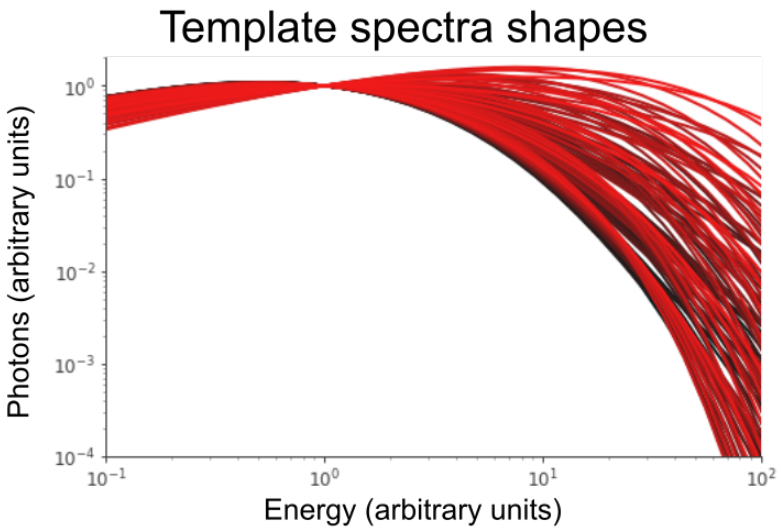

Figure 4: Template spectra shapes as generated by Komrad.

2.1.2 Noise and Randomness

In order to simulate the appearance of real GRBs, the synthetic spectra were modified in three ways. The first modification was the addition of background photons. When taking measurements in space, background radiation from different sources can interfere with the primary signal being observed. These background photons are more prevalent in the low energy band, and become less common at higher frequencies. To simulate this, background photons in the shape of a power law were added to the synthetic spectra.

Another issue that may arise when attempting to measure individual photons is that

scatterings or other interactions may occur near the lens of the telescope. Space telescopes are designed to mitigate these random elements, but are unable to eliminate them, which leads to a level of randomness in the data obtained. This is simulated by adding small amounts of random noise to the spectra.

The impact of these noise and background photons was varied using the Signal-to-Noise Ratio (SNR) parameter. For higher values of SNR, more photons were added to the synthetic spectrum, diminishing the impact of the discrepant photons on the shape of each spectrum.

Lastly, another factor to account for is that space telescopes are unable to measure every photon at every energy. The Gamma-ray Burst Monitor on the Fermi Gamma-ray Space Telescope has a range from 8 keV to 30 MeV, but it is also necessary to account for the telescope being more or less sensitive in certain energy ranges [13]. In this study, response data from two of the nodes on the Gamma-ray Burst Monitor was used. The majority of simulations were run using the response data of the fifth node, N4, but some data was also obtained using the node response of the first node, N0. Differences between the sensitivities of each node in certain energy bands can affect the overall shape of the spectrum, as seen in figure 5.

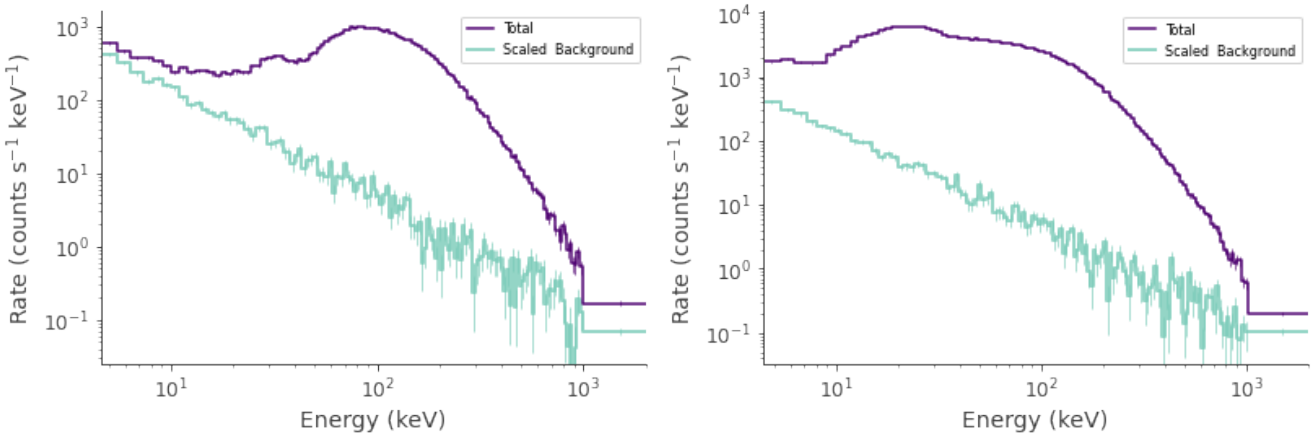

(a) N0 response for R = 30, $Y_R = 0.8$, $\tau\theta = 5$.

(b) N4 response for R = 30, $Y_R = 0.8$, $\tau\theta = 5$.

Figure 5: Comparison between the responses of two nodes, N0 and N4, where the purple curves represent the spectra and the light green curves represent background photons.

2.2 Interpretation of Synthetic Spectra

After the synthetic spectra were modified, the Band function was fit to them in order to find an expression that defined their shape. Data was then obtained by creating 100 synthetic spectra with static values of $\tau\theta$ and Y_R while varying R and subsequently observing the changes in the α parameter of the Band function. The relationship between R and α was plotted and fitted with best fit curves using regression analysis. Lastly, the original spectra without noise were plotted against their respective Band functions to determine the accuracy of the Band fit.

2.2.1 Data Obtained

Because photon measurements are more accurate in the lower energy band, it was decided that this study would focus on changes in α between 100 spectra. The Komrad parameter R was arbitrarily chosen as the main variable for the study and varied from the minimum value 30 to the maximum value 300 across the 100 synthetic spectra generated. Two values 0.8 and 1.5 were used for Y_R in order to observe the effect of a positive or negative gradient on the α value, and $\tau\theta$ was kept at 5 for all spectra. Additionally, the model was run for SNR values of 1000, 100 and 10 respectively to monitor the impact of noise on the results.

For each measurement, a plot was made comparing the initial spectra pre-noise to the fitted curves generated by the Band function. These plots included spectra for R = 30, R = 165 and R = 300 in order to compare the accuracy of the Band fit across the range of R. The background radiation function was also included in the plot for the purpose of visualising the level of background photons added to each energy band. It is worth noting that this plot does not merely represent photon count per unit energy E. Even if there are many more photons in the lower energy band, they may only represent a small fraction of the total photon energy of the spectrum, which can be misleading. This is prevented by multiplying the spectra by E^2 in order to obtain a y-axis of photon counts multiplied by E, which more accurately represents the distribution of photon energies.

2.2.2 Statistical Analysis

Regression analysis was used to generate lines of best fit for the correlation between R and α across the 100 spectra. The correlation of the best fit function to the obtained data was determined by calculating the coefficient of determination r^2, with $r^2 = 1$ indicating a good correlation and $r^2 = 0$ indicating no correlation.

In a data set, the values of the dependent variable are labelled y_i, while the values produced by the best fit function are labelled f_i. Further, the mean of all y_i is labelled $\bar{y}$. Using these numbers, the sum of squares SS_{tot}, representing overall variance, and sum of squares residuals SS_{res}, representing the discrepancy between data and best fit curve, are calculated in accordance with equations (2) and (3). [14]

$$SS_{tot} = \sum_i (y_i - \bar{y})^2 \tag{2}$$

$$SS_{res} = \sum_i (y_i - f_i)^2 \tag{3}$$

These sums are then used to calculate r^2 according to equation (4). [14]

$$r^2 = 1 - \frac{SS_{res}}{SS_{tot}} \tag{4}$$

3 Results

Figures 6 and 7 show the main data gathered from synthetic spectra for 3 different SNR values and 2 values of Y_R. In figure 6, the Band function parameter α is plotted against the Komrad parameter R along with two best fit curves for each figure (see appendix for individual graphs). The best fit curves describe a quadratic relationship for $R < 100$ and a linear relationship for $R \geq 100$, with r^2 for each curve printed in table 1. In the second and third rows of figure 6, α values for the lowest values of R are below the window of the graph, altering the quadratic fit.

Figure 7 shows a selection of pre-noise spectra corresponding to the plots in figure 6 and superimposes the Band function fits for each spectrum for comparison. The vertical dashed lines represent the observational window in which the spectra are fitted, and the dashed and dotted line represents the background radiation.

Figures 8 and 9 show adjacent results that are relevant. Figure 8 is another plot of α to R, but for an SNR of 10^5, essentially making random noise negligible. Figure 9 shows results from synthetic spectra generated using the response of the N0 node as opposed to the N4 node which was used to obtain all other data.

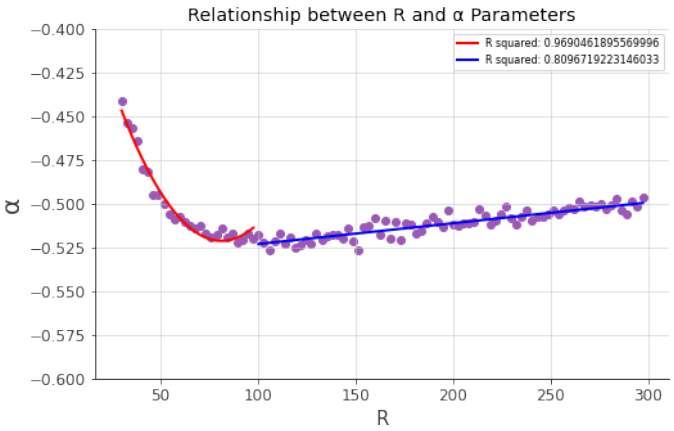

(a) Plot of α vs. R for SNR = 1000 and $Y_R = 0.8$.

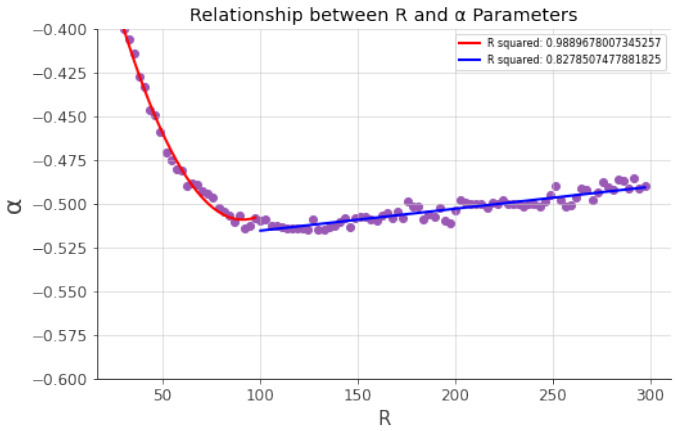

(b) Plot of α vs. R for SNR = 1000 and $Y_R = 1.5$.

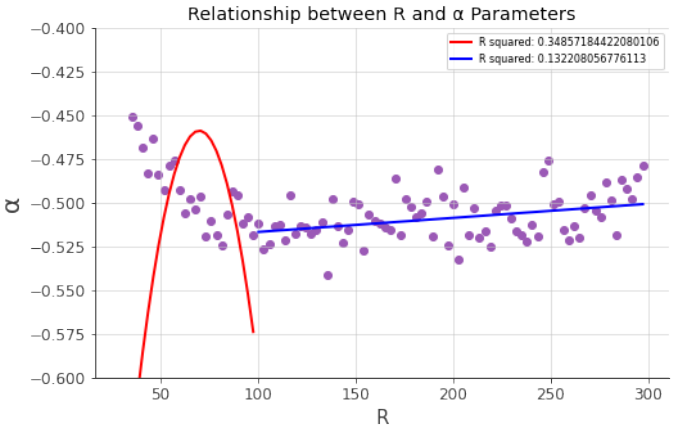

(c) Plot of α vs. R for SNR = 100 and $Y_R = 0.8$.

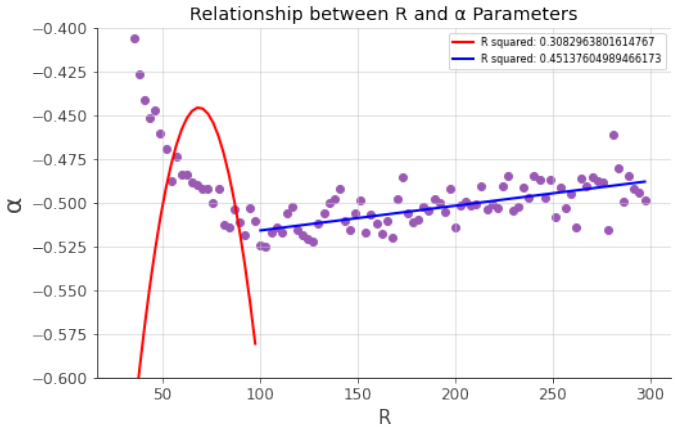

(d) Plot of α vs. R for SNR = 100 and $Y_R = 1.5$.

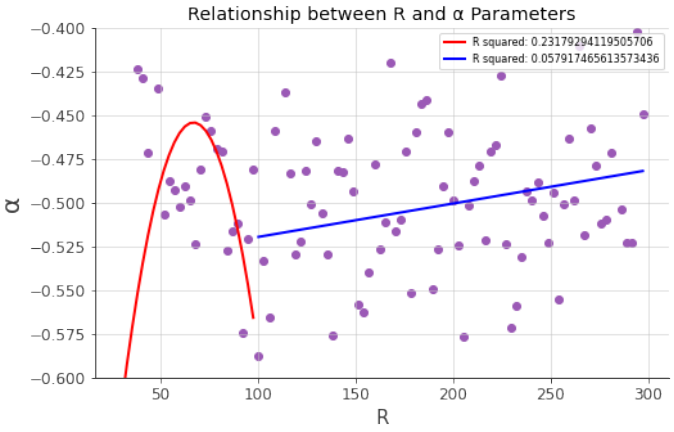

(e) Plot of α vs. R for SNR = 10 and $Y_R = 0.8$.

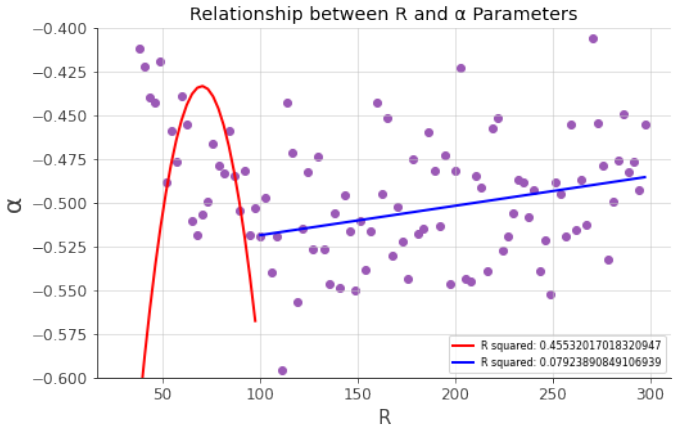

(f) Plot of α vs. R for SNR = 10 and $Y_R = 1.5$.

Figure 6: Combined plots of R vs α for three values of SNR and two values of Y_R with $\tau\theta = 5$ across all spectra.

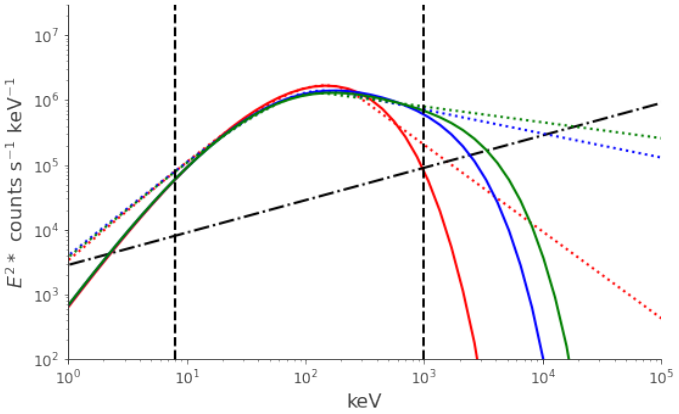

(a) Spectra vs. Band for SNR = 1000 and $Y_R = 0.8$.

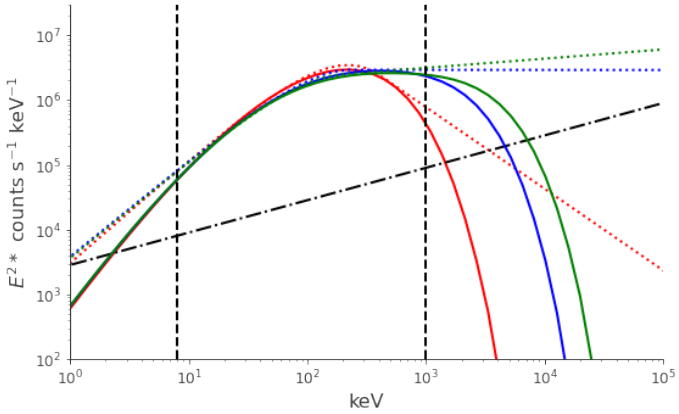

(b) Spectra vs. Band for SNR = 1000 and $Y_R = 1.5$.

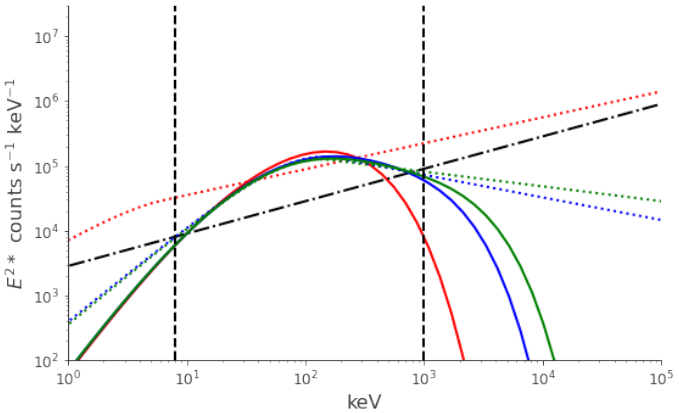

(c) Spectra vs. Band for SNR = 100 and $Y_R = 0.8$.

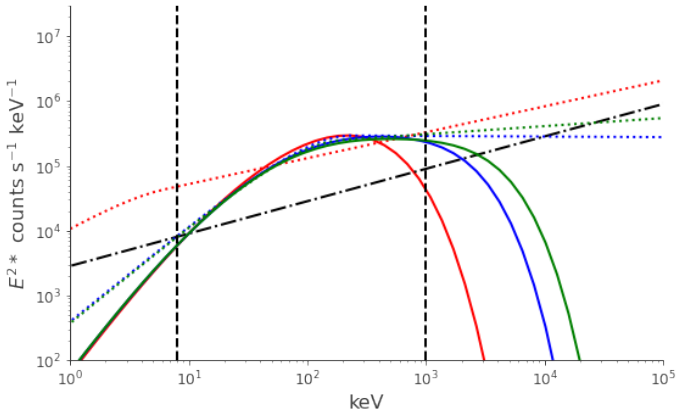

(d) Spectra vs. Band for SNR = 100 and $Y_R = 1.5$.

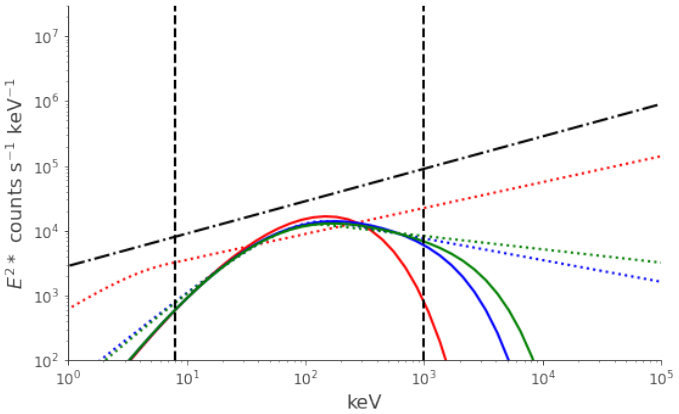

(e) Spectra vs. Band for SNR = 10 and $Y_R = 0.8$.

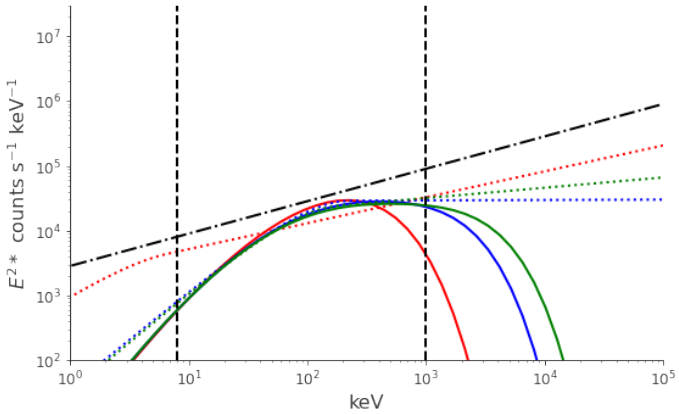

(f) Spectra vs. Band for SNR = 10 and $Y_R = 1.5$.

Figure 7: Combined plots showing comparisons between the synthetic spectra (coloured lines) and Band function fits (dotted lines). R values from left to right: Red = 30, Blue = 165 and Green = 300.

Table 1: r^2 values for each best fit curve in every set of parameters.

	r^2 for the quadratic fit	r^2 for the linear fit
SNR = 1000, $Y_R = 0.8$	0.97	0.81
SNR = 100, $Y_R = 0.8$	0.35	0.13
SNR = 10, $Y_R = 0.8$	0.23	0.05
SNR = 1000, $Y_R = 1.5$	0.99	0.83
SNR = 100, $Y_R = 1.5$	0.31	0.45
SNR = 10, $Y_R = 1.5$	0.46	0.08

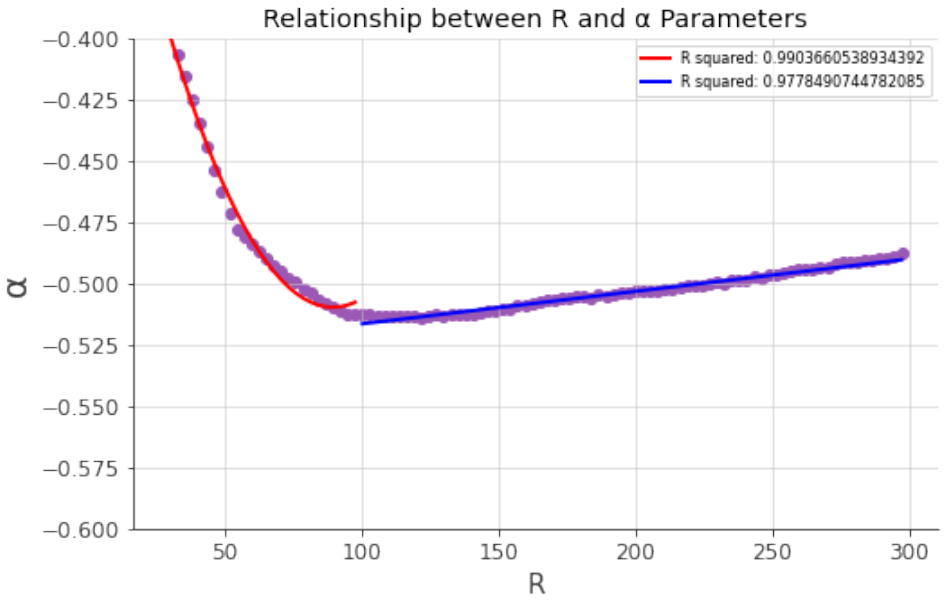

Figure 8: Correlation between R and α in spectra generated at $Y_R = 1.5$ and $\tau\theta = 5$ for SNR = 10^5.

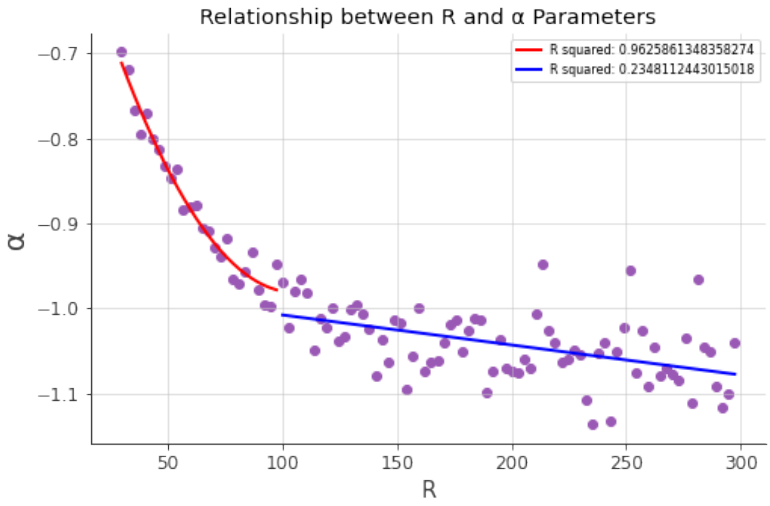

(a) α vs. R at SNR $= 100$, $\mathrm{Y_R} = 0.8$ and $\tau\theta = 5$.

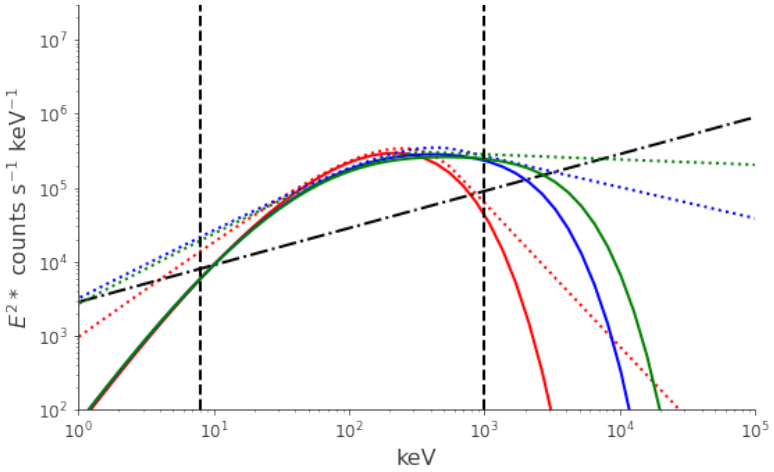

(b) Spectra vs. Band at SNR $= 100$, $\mathrm{Y_R} = 0.8$ and $\tau\theta = 5$.

Figure 9: Data generated from the N0 response.

4 Discussion

Figures 6 and 8 indicate that there is a clear relationship between R and α. For lower values of R, the decline of the spectrum at high energies is within the observational range of the telescope, meaning that the Band function is able to account for it. As R ranges from 30 to 100, this decline becomes less apparent, resulting in a rapid decrease in α. However, once R approaches 100, this decline disappears from view. As R increases from that point, there is a gradual, seemingly linear increase in α. This relationship was fit with a quadratic function for $R < 100$ and a linear function for $R > 100$. An issue with this fit is that it does not account for the smooth shift from a quadratic relationship to a linear one. However, it may be possible to obtain a more accurate fit by using polynomial interpolation to smoothly incorporate the two separate components. Further, the difference between $\mathrm{Y_R}$ values of 0.8 and 1.5 was subtle, due to the gradient of the spectrum primarily affecting the β parameter of the Band function. The main difference was that the range of α was expanded to approximately -0.4.

In figures 6 and 7, the first α values are significantly lower than all the others for SNR values under 1000, resulting in incorrect best fit and Band function curves. This is due to a quirk particular to the N4 response of the Fermi telescope, where there is a bump

in observed photons in the $10 - 100$ keV range, see figure 5. This gives a high number of detected photons in a range that is typically well below the peak of the spectrum. When combined with low values of R leading to a visible decline in photons, this bump interferes with the perceived shape of the spectrum, forcing the Band function to put E_0 outside the observational range of the telescope and giving very low values of α. Spectra with high values of SNR are not affected by this because there are enough photons in all energy bands to effectively "drown out" the interference of this bump.

As shown in figure 9, spectra generated by the N0 node do not share this flaw. However, the N0 response has a bump around the 100 keV range that affects the ability of the Band function to accurately determine α, see figure 5. This can both be seen in the lack of a linear increase in α for $R > 100$ and in the Band function curves not being aligned to the spectra in figure 9. As both the N4 and N0 nodes have flaws that impact the ability to see a correlation between R and α, it is difficult to determine which one was most accurate. In future research, it may be possible to use the responses of additional nodes to find a more general correlation that holds true for all of them. Such a correlation could be used to ascertain information about the temperature of the subphotospheric shocks that gave rise to GRBs based only on the shape of their spectra.

However, an issue with finding relationships such as these is that they are highly theoretical. The scatter plots in figure 6 and r^2 values in table 1 indicate that the subtle correlation between R and α becomes almost invisible at lower and more realistic SNR values, meaning that there is no way to verify this relationship with current technology. One aspect of these results that does lend the model credibility, however, is that the α values for synthetic spectra stay within the range of most common α values in real GRBs.

4.1 Conclusion

In conclusion, a relationship can be seen between the Komrad parameter R and the Band function parameter α due to the varying visibility of the decline in photon energies. The relationship has been defined as a quadratic decrease followed by a linear increase, but this fit is considered suboptimal due to its disjointed nature. Additionally, individual differences between the responses of different nodes on the Fermi Telescope significantly alter the ability of the Band function to fit the similar spectra, thus affecting any observed correlations between parameters to an unclear degree. Future studies may be required to look into the responses of more nodes to find a common correlation that holds between them and define this relationship in a more accurate way, potentially allowing for the inference of more GRB properties from the perceived shapes of their spectra.

References

[1] Iyyani S. Photospheric emission in gamma ray bursts: Analysis and interpretation of observations made by the Fermi gamma ray space telescope. Department of Physics, Stockholm University; 2015.

[2] Meszaros P. Gamma-ray bursts. Reports on Progress in Physics. 2006;69(8):2259.

[3] Kitchin CR. Stars, nebulae and the interstellar medium: observational physics and astrophysics. CRC Press; 1987.

[4] Blinnikov S, Kozyreva A, Panchenko I. Gamma-ray bursts: when does a blackbody spectrum look non-thermal? Astronomy Reports. 1999;43(11):739–747.

[5] Samuelsson F. Multi-messenger emission from gamma-ray bursts. KTH Royal Institute of Technology; 2020.

[6] Blinnikov S. Cosmic gamma-ray bursts. Surveys in High Energy Physics. 2000;15(1-3):37–74.

[7] Haug E, Nakel W. The elementary process of bremsstrahlung. vol. 73. World Scientific; 2004.

[8] Wiedemann H. Synchrotron radiation. In: Particle Accelerator Physics. Springer; 2003. p. 647–686.

[9] Williams B. Compton scattering: the investigation of electron momentum distributions; 1977.

[10] Levinson A. Observational signatures of sub-photospheric radiation-mediated shocks in the prompt phase of gamma-ray bursts. The Astrophysical Journal. 2012;756(2):174.

[11] Shirk DG. A practical review of the Kompaneets equation and its application to Compton scattering. 2006.

[12] Pe'er A. Physics of gamma-ray bursts prompt emission. Advances in Astronomy. 2015;2015.

[13] Fermi Spacecraft and Instruments. The United States Government; 2017. Available from: `https://www.nasa.gov/content/goddard/fermi-spacecraft-and-instruments`.

[14] Draper NR, Smith H. Applied regression analysis. vol. 326. John Wiley & Sons; 1998.

A Individual Graphs

Below are the individual graphs used for figures 7-8 with associated data.

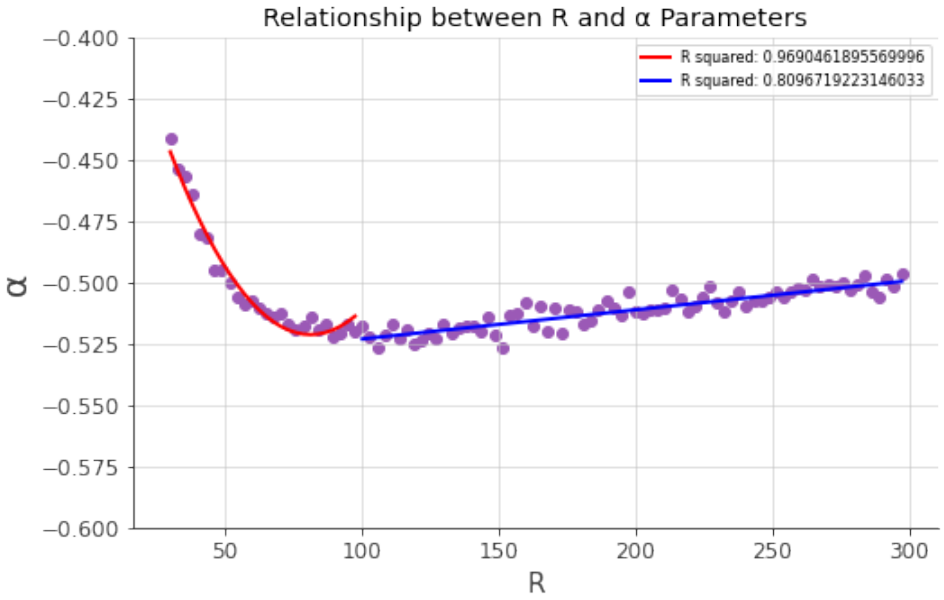

Figure 10: Correlation between R and α in spectra generated at $Y_R = 0.8$ and $\tau\theta = 5$ with SNR = 1000.

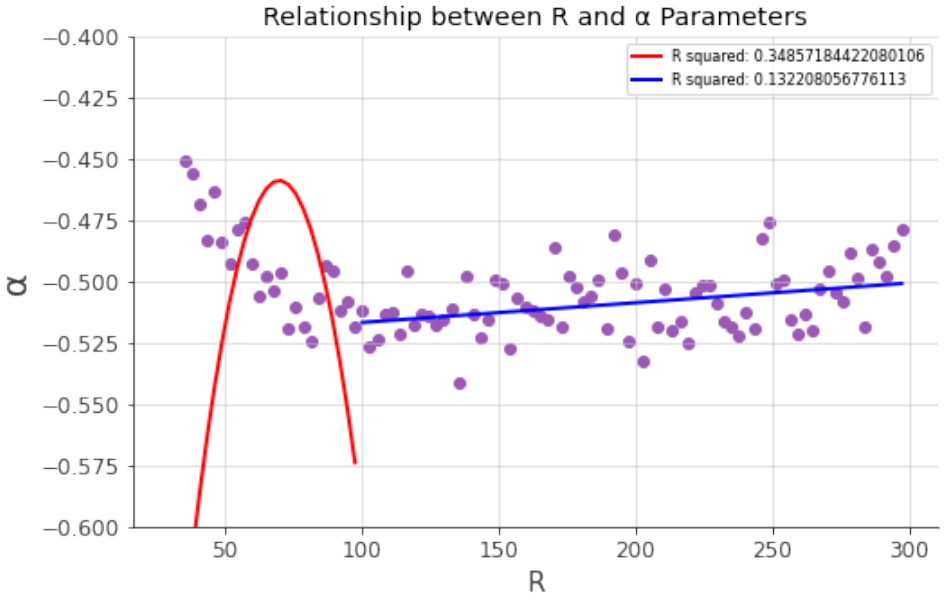

Figure 11: Correlation between R and α in spectra generated at $Y_R = 0.8$ and $\tau\theta = 5$ with SNR = 100.

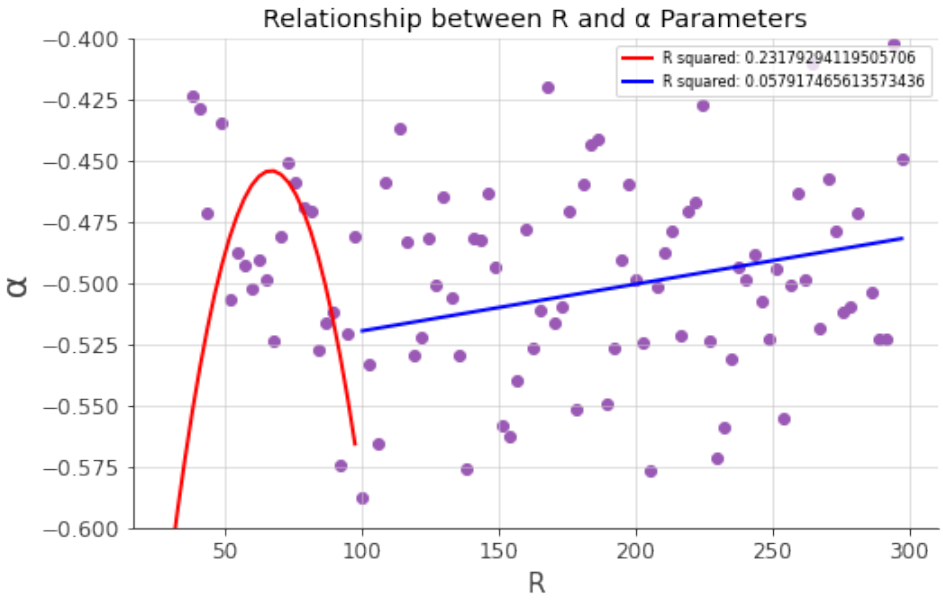

Figure 12: Correlation between R and α in spectra generated at $Y_R = 0.8$ and $\tau\theta = 5$ with SNR = 10.

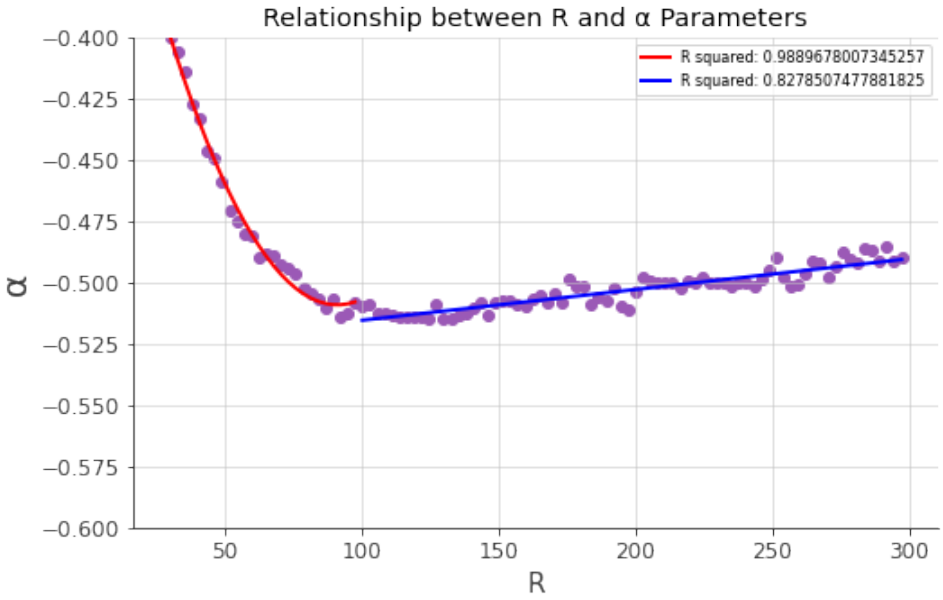

Figure 13: Correlation between R and α in spectra generated at $Y_R = 1.5$ and $\tau\theta = 5$ with SNR = 1000.

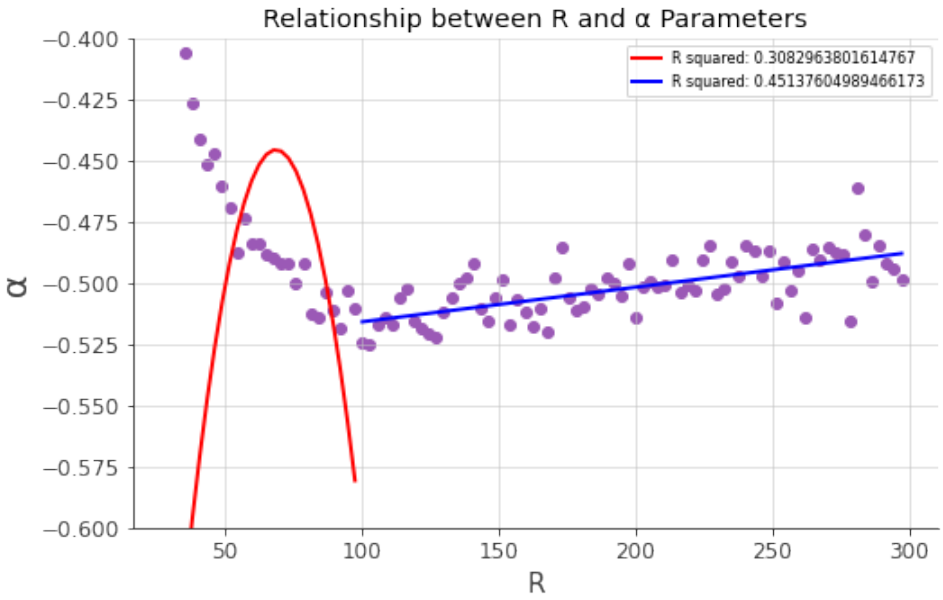

Figure 14: Correlation between R and α in spectra generated at $Y_R = 1.5$ and $\tau\theta = 5$ with SNR = 100.

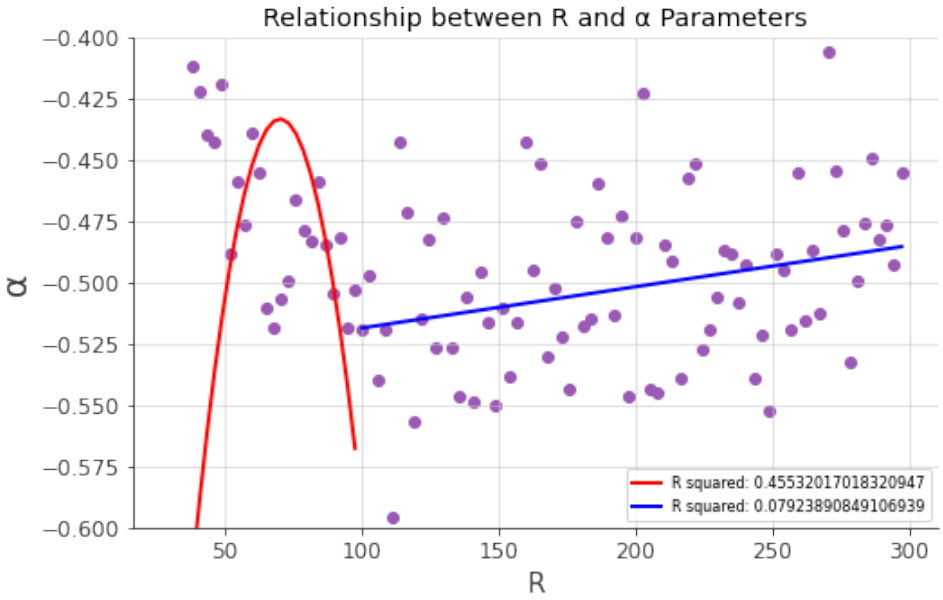

Figure 15: Correlation between R and α in spectra generated at $Y_R = 1.5$ and $\tau\theta = 5$ with SNR = 10.

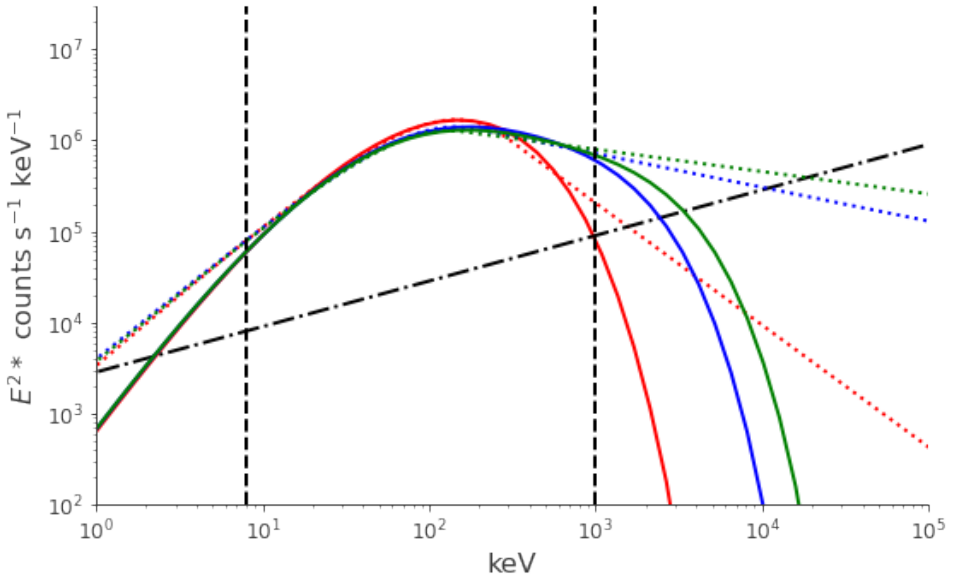

Figure 16: Spectra and Band function curves compared at $Y_R = 0.8$ and $\tau\theta = 5$ with SNR = 1000.

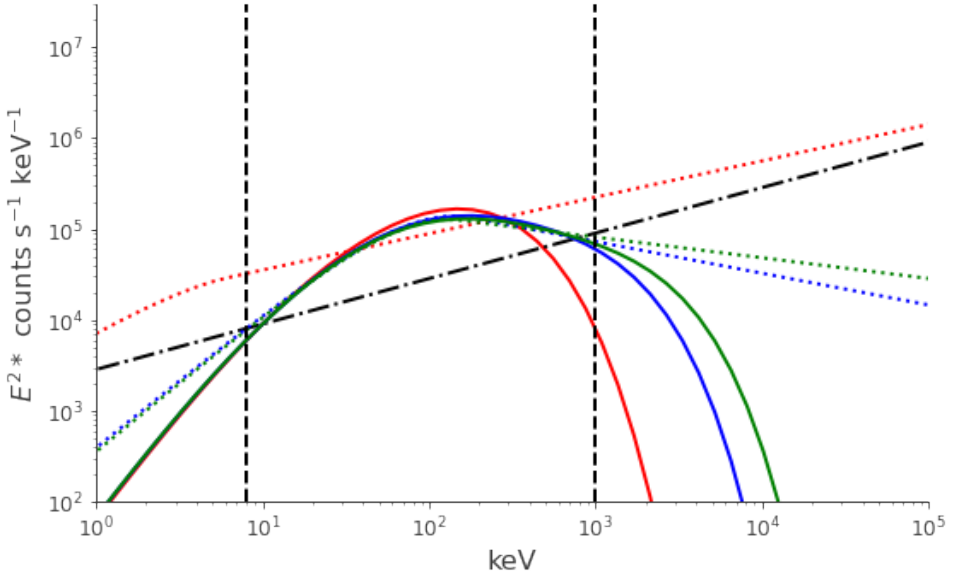

Figure 17: Spectra and Band function curves compared at $Y_R = 0.8$ and $\tau\theta = 5$ with SNR = 100.

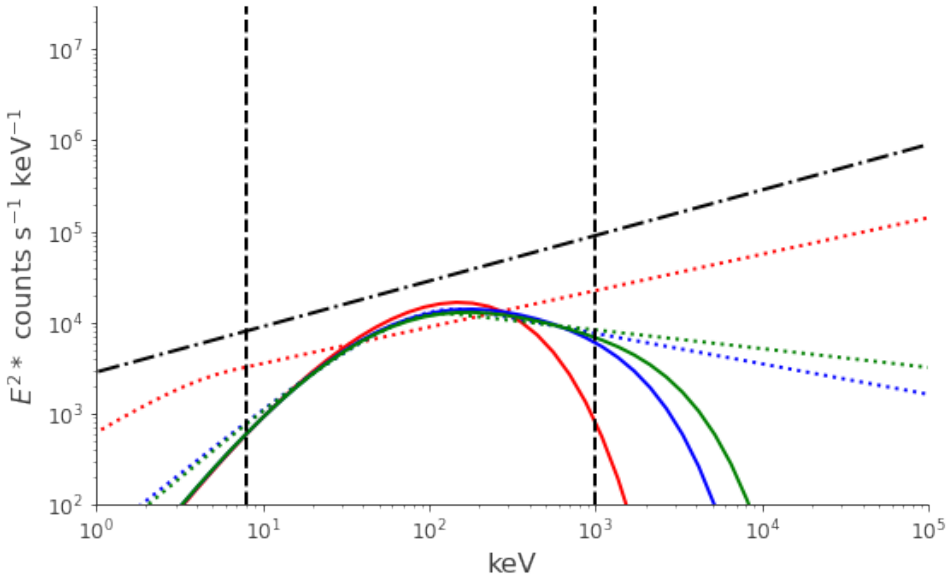

Figure 18: Spectra and Band function curves compared at $Y_R = 0.8$ and $\tau\theta = 5$ with SNR = 10.

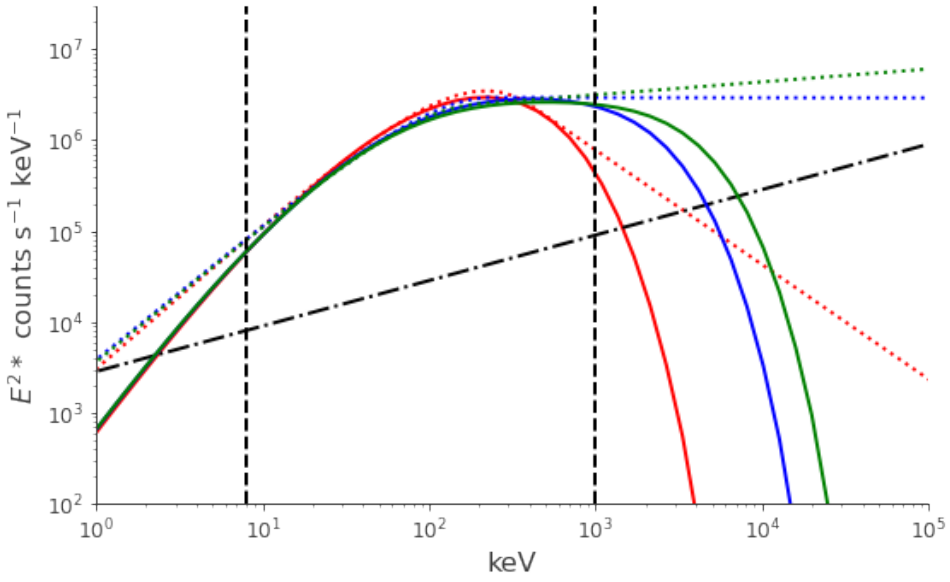

Figure 19: Spectra and Band function curves compared at $Y_R = 1.5$ and $\tau\theta = 5$ with SNR = 1000.

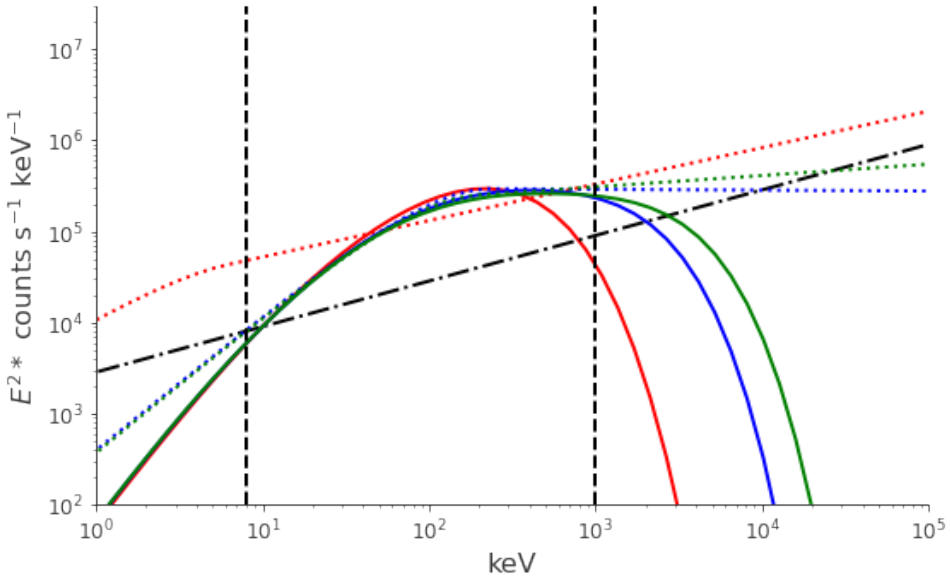

Figure 20: Spectra and Band function curves compared at $Y_R = 1.5$ and $\tau\theta = 5$ with SNR = 100.

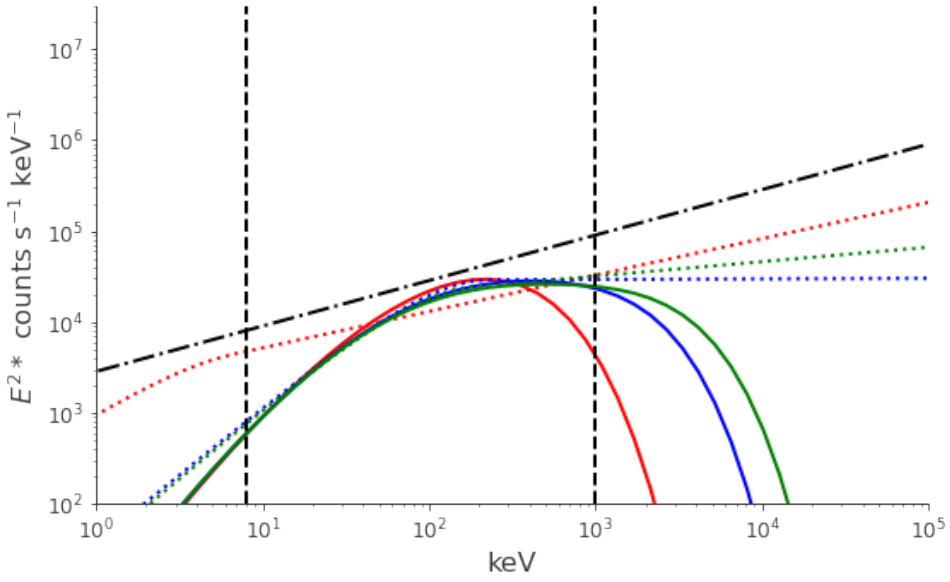

Figure 21: Spectra and Band function curves compared at $Y_R = 1.5$ and $\tau\theta = 5$ with SNR = 10.